Romanian Reports in Physics, Vol. 64, Supplement, P. 1355–1372, 2012

Dedicated to Professor Ioan-Iovitz Popescu's 80th Anniversary

CONTRIBUTIONS TO THE SPECTRAL DIAGNOSTICS OF THE TEMPORAL AFTERGLOW PLASMAS

A. SURMEIAN

National Institute of Lasers, Plasma and Radiation Physics, 077125 Bucharest- Magurele, Romania
E-mail: surmeian@infim.ro

Received April 26, 2012

Abstract. The paper is a review of the recent spectroscopic studies on the temporal afterglow plasma of short high voltage pulsed discharges in noble gases and of the original diagnostic methods for afterglow plasma resulted from these studies. Besides the experimental investigations, simple theoretical methods applied, contributed to the identification of the complex processes occurring in these plasmas.

Key words: temporal afterglow plasma, pulsed discharge, spectral diagnostics.

1. INTRODUCTION

It is already well known that in the afterglow plasma, also known as remote plasma, the external electromagnetic fields that sustained the plasma glow are absent or insufficient to maintain the discharge. A plasma afterglow can either be a temporal, due to an interrupted (pulsed) plasma source, or a spatial one, due to a distant plasma source. Depending on the gas composition, super-elastic collisions may continue to sustain the plasma in the afterglow for a while by releasing the energy stored in the metastable states of the atoms and molecules in the plasma.

The purpose of this paper is to briefly review the spectroscopic studies on the temporal afterglow plasma mainly the afterglow of the short high voltage pulsed discharges in noble gases.

Since the pulsed plasmas are widely used in various technological applications [1, 2], the understanding of the phenomena-taking place in afterglow phase of the discharge makes possible the optimization of the operation conditions and improvement of the technical parameters. Is also worth noting that the study of the afterglow of pulsed discharge plasma is of great scientific interest; since after switching off the discharge, various relaxation phenomena governed by collisions, radiation, recombination, etc, proceed during the plasma de-ionization, being unobserved in the active phase. This is why afterglows are successfully used for measurements of the rate coefficients of elementary processes and effective lifetimes of various excited states [3].

The plasma chemistry in the afterglow is significantly different from the plasma glow. The superelastic collisions continue to sustain the plasma after the end of the current pulse by releasing the energy stored in metastable atoms and molecules. The metastables are produced during the pulse current by electron impact excitation from the ground state and loosed by electron impact quenching, quenching by collision with noble gas neutral atoms and by diffusion to the walls. More efficiently they are produced as a result of the electron-ion recombination and can act as an important energy reservoir for subsequent Penning ionization of gas impurities or minority admixtures [4–7]. Thus the excited metastable atoms play a key role in plasma ionization and sustainment mechanisms in pulsed GDOES and GDMS analytical systems

2. EXPERIMENTAL SETUP

As we have already mentioned, the aim of this paper is to review the spectroscopic studies on the afterglow plasma of the short high voltage pulsed discharges in noble gases in order to obtain insight over the processes occurring in the plasma.

The experimental setup shown in Fig. 1 and used in our experiments was especially designed to investigate the spectral emission of the afterglow plasma of high-current-density pulsed discharges in a hollow cathode configuration [4, 8]. The discharge tube, which was made of glass, contained a cylindrical hollow titanium cathode (15 mm in length and 4 mm in diameter), and the anode consisted of a stainless steel ring (4 mm in diameter) placed 2 mm from the cathode. Short high-current pulses were produced by discharging a storage capacitor through a rotary spark gap with a commutation time of less than 10 ns [1]. At a filling gas pressure of 1–5 Torr, peak current pulses of between 20 and 100 A were obtained with a duration of 60 ns (at half-width), depending on the charging voltage of the main capacitor. The optical emission measurements are made with a detection system syncronized with the current pulse period.

The time-resolved emission signals, giving the population of the excited levels, were measured with a 1 m Jarrell ash monochromator equipped with a EMI photomultiplier. The PMT output was fed into a 500 MHz digital storage oscilloscope (TECTRONIX 54542C Digitizing Oscilloscope), which was set to average the signal continuously over 256 successive discharge pulses. The leading edge of the applied voltage synchronized the signal profiles. For recording with temporal resolution emission spectra of the species present in the plasma a system with an electronic temporal gate with variable duration and delay related to the applied pulse has been used.

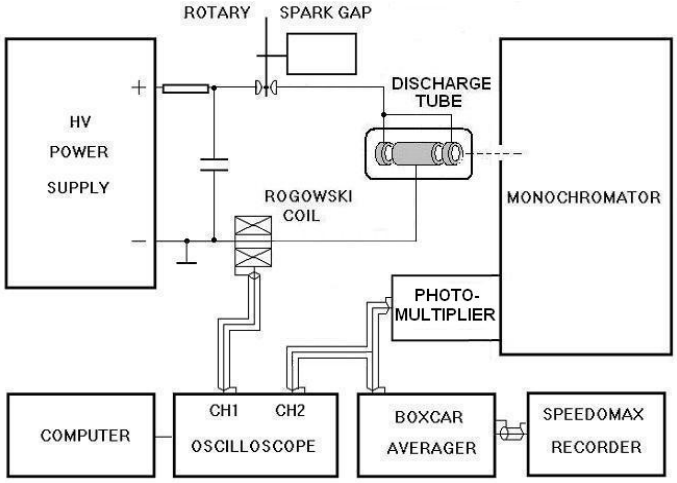

Fig. 1 – Experimental set up with measuring system for temporal resolution spectral analysis.

3. RESULTS AND DISCUSSIONS

3.1. THE TEMPORAL PROFILES OF THE NOBLE GAS ATOMIC LINES AND THE BENEFITS IN THE DIAGNOSTICS OF THE AFTERGLOW PLASMAS

The temporal evolution of the light emission of Argon atom and ions at 415.8 nm, 337.6 nm, 334.4 nm, Neon atom at 585.2 nm, Hydrogen H_α, H_β, H_γ transitions, hydrogen being as impurity in noble gases in a short pulsed (100 ns) hollow cathode high voltage discharge shows a long duration of the emission light (> 100 μs) after the end of the discharge pulse (Fig. 2).

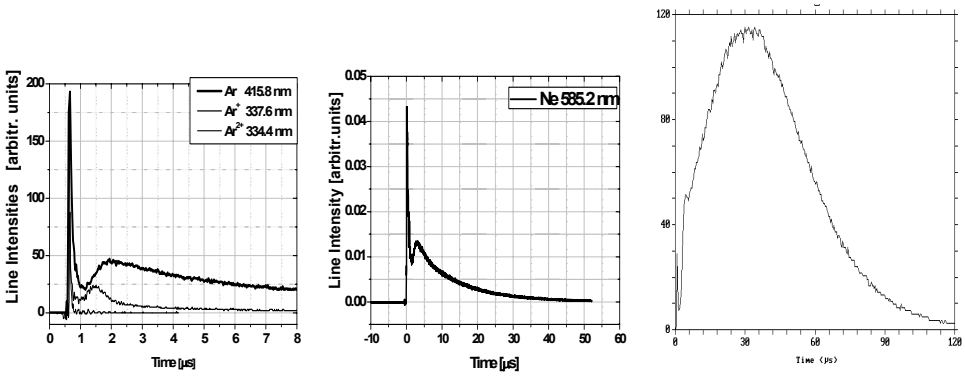

Fig. 2 – The temporal evolution of the light emission of Ar, at 415.8 nm, Ar^+ 337.6 nm, Ar^{++} 334.4 nm, Ne at 585.2 nm, and H_β, hydrogen being as impurity in Neon.

As it can be seen in the figure the relative intensity of the emission lines during the current pulse and afterglow varies from line to line and more than that their afterglow behavior varies significantly from line to line.

From the observed time variation of emission lines and from the atomic spectra recorded with electronic gate positioned during the current peak and in the afterglow, Fig. 3, we tried to elucidate the mechanism responsible for the population of the atomic levels during the discharge pulse and during the afterglow.

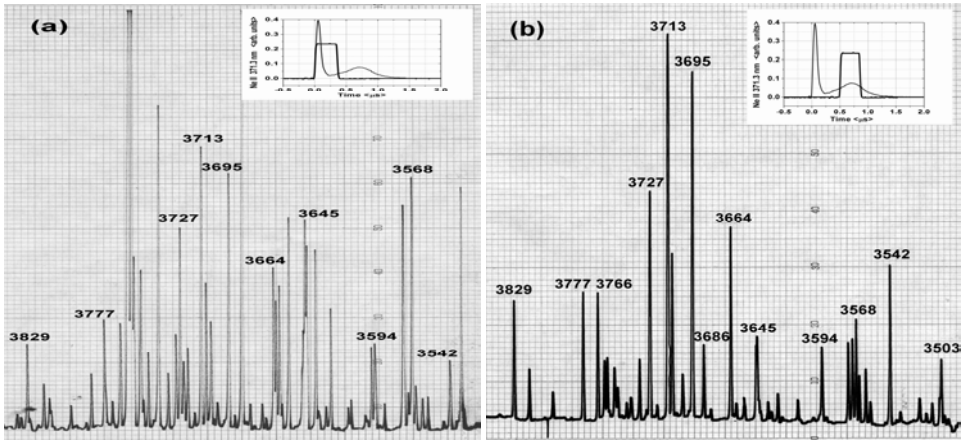

Fig. 3 – The Neon spectra recorded during: a) the current pulse; b) during the afterglow.

The variation in the relative population of excited states during the pulse and afterglow regions indicates that the excitation mechanism differs during these two periods. The large initial peak after discharge initiation corresponds to the electron impact excitation. Free electrons are generated during the current electrical discharge and undergo several collisions with the particles in the discharge. Thus ground state noble gas atoms are excited to high energy levels followed with the spontaneous radiative relaxation. The afterglow is indicative of a recombination process. The time gap between the initial peak and the afterglow may represent the initial rapid cooling of the electrons. As the electrons lose energy in inelastic collisions, the conditions become favorable for recombination [9] and the afterglow intensity rises.

Our spectroscopic studies on the light emission from pulsed high voltage discharges proved that the long afterglow shape of the temporal evolution of the atomic spectral lines may be of interest for some applications. Thus by focusing a limited zone of about 10% of the discharge cross section on the square entrance slit (100×100 μm) of the Jarrell-Ash monochromator, the acoustic modulation of the afterglow light were observed. The acoustic modulation was observed for all lines of the excited species present in the pulsed discharge afterglows in neon and in

helium and also in atomic hydrogen present as an impurity in the neon and helium afterglows. Figures 4a and b present the acoustic modulation of the afterglow light of the H_α line in neon (5 Torr) and in helium (12 Torr) afterglows, respectively, hydrogen being present as an impurity in the neon and helium discharges.

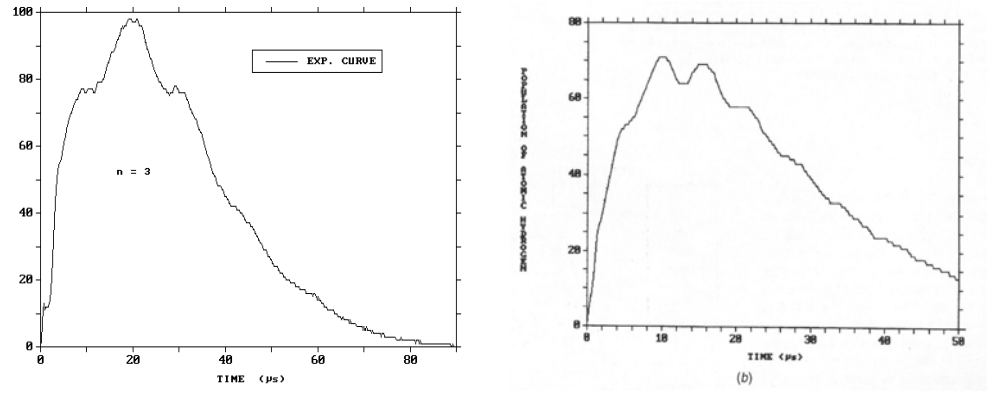

Fig. 4 – Ultrasonic standing waves in H_α in Neon and Helium afterglow.

In view of the small capacity of low-pressure gases, a substantial heating of the neutral gas has to be expected at still lower breakdown powers because only a small portion of the energy coupled into the gas discharge can be radiated away. At early times, thermal expansion and shock waves will contribute to the heat dissipation, whereas later on, cooling will proceed mainly by thermal conduction in the gas to the walls of the discharge tube. The temperature decay is then a function of the initial temperature distribution, the tube geometry and the thermal properties of the gas. Weakly damped, the shock wave generated by the pulsed breakdown propagates in the gas and affects all phenomena, which are directly dependent upon the densities either of the charged or of the neutral constituents in the plasma. The acoustic modulation of the afterglow light of the Balmer lines of atomic hydrogen impurity, which have a particular shape and size in the afterglow of the neon or helium pulsed discharge, Fig. 1 has been used to determine acoustic wave's frequency, the velocity of sound and the gas temperature [10].

The long afterglow and the shape of the hydrogen lines in neon and helium discharges are due mainly to the dissociative recombination processes of the hydrogen molecular ion produced by Penning reaction with neon or helium metastables [4]. The local variation in ion concentrations produced by the shock waves during the pulsed discharge affects the total rate of the recombination process and, finally, the variation of line intensities. The depth of modulation superimposed on the afterglow light are strongly dependent on the energy in the discharge pulse and on the gas pressure. The measurements made as a function of position in the discharge (from the centre of the tube to the walls) proved that the

oscillations observed correspond to the lowest harmonic of the standing waves. The acoustic modulations on spectral lines are present whatever the position of the light detection would be in the discharge. The only variable parameter is the intensity of the modulation (large at the center, weak at the walls). Concerning the wavefrequency, as it can be seen in Fig. 3, the waves are strongly damped within a few oscillations and the frequency does not change significantly during the afterglow, but rather is dependent on the nature of the gas; the period for neon is longer than that for helium, in accordance with their relative atomic masses. Moreover, in the case of argon, which has the relative mass 40, the period of the shock waves exceeds the entire duration of the afterglow (150 μs) and the light modulation cannot be observed. Another observation revealed that the wave period became larger as the discharge tube increased.

Using a mathematical artifice we processed the modulations of the Balmer lines (Fig. 3), in order to determine the gas temperature in the discharge afterglow. Thus, the ondulations were better revealed when we have fitted the light signal by a 9th order polynom (dashed curve – Fig. 5a). The fitting curve has been extract from the experimental signal and we have got the clean oscillations presented in Fig. 5b. From Fourier spectrum of these oscillations (Fig. 5c), we obtained the frequency of the pressure wave in neon.

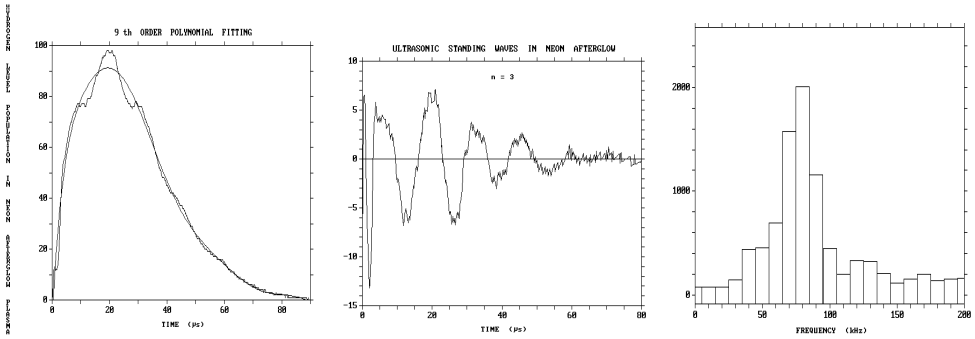

Fig. 5 – The fitted light signal by a 9^{-th} order polynom (a); the obtained clean oscillations (b); the Fourier spectrum of the oscillations (c).

In order to evaluate the gas temperature we used the expressions of the sound velocity [11, 12] $v_s = 2\pi\nu_s / k_s = (\gamma kT/m)^{1/2}$, where ν_S and k_S are the frequency and the corresponding wave number of the sound, $\gamma = c_p / c_V$ = ratio of specific heats, k = Boltzmann constant, T = gas temperature, and m = mass of the gas atom. In addition, we shall consider that the observed oscillations correspond to the lowest harmonic, thus kR = 3.83 [12], where R = radius of the discharge tube (in our experiment R = 9 mm). We applied these relationships to the afterglows of neon (5 Torr) and helium (12.5 Torr) having about 10^{-2} Torr hydrogen impurity. Under these conditions, we get from the Fourier spectrum a value of about 80 kHz

for neon and 160 kHz for helium. The corresponding sound velocities are about 1200 m/s in neon and 2400 m/s in helium. Taking further $\gamma = 1.67$, we obtain finally an average gas temperature of about $T = 2100$ K in neon and 1700 K in helium afterglow [13].

In our experimental conditions of high voltage pulsed discharges the emission lines of the atoms and ions in the pulsed plasma are Doppler broadened; the Doppler width of the spectral lines beeing dependent on the gas temperature of the plasma: $\Delta\lambda_D = \frac{\lambda_0}{c}\sqrt{\frac{2kT}{m}}$. Thus the determination of the Doppler width of the atomic and ionic lines in the pulsed discharge using the measurements of gas temperature from the shock waves, is a simple and easy method which avoids all the complications of the high resolution spectroscopy methods used until now and allows the use of the hollow cathode pulsed discharges as spectral source for temporal resolution spectroscopy [14, 15, 16].

3.2. THE EVIDENCES OF THE RECOMBINATION PROCESSES OCCURRING IN THE PULSED HIGH VOLTAGE AFTERGLOW PLASMAS; BENEFITS FOR THE DIAGNOSTICS

Besides the characteristic temporal profile of the spectral lines in the afterglow, we reported another two spectral evidences proving that the recombination process dominates the population of the energy levels of atoms in afterglow plasma. One of them consisted in testing the so-called afterglow quenching effect [17]. It is well known that the rates of various electron-ion recombination processes decrease with increasing electron energy. It is obvious that if the afterglow radiation is due to recombination processes, increasing electron energy in a way or another at a time may produce the quenching of the afterglow radiation in that time.

The original electric set-up we used emphasized the effect of the "afterglow quenching". A short accelerating voltage applied between the main electrodes during the afterglow has been achieved by inserting a ferrite coil in the external circuit of the discharge, thus obtaining an oscillating discharge mode consisting in short and delayed alternating pulses. The experiments have been carried out in pure noble gases and in mixture noble gases with hydrogen traces. We present below the afterglow quenching of H_β line in a mixture of 5 Torr of neon and 0.1 Torr of hydrogen (Fig. 6).

The drastic afterglow quenching in atomic hydrogen Balmer lines during the second positive pulse due to a significant electron heating in the afterglow plasma (the first positive pulse corresponds to the discharge phase and just "starts" the afterglow plasma while the negative pulse is not relevant for plasma heating) proves the main role of the dissociative recombination processes in the population mechanism of atomic hydrogen levels [4].

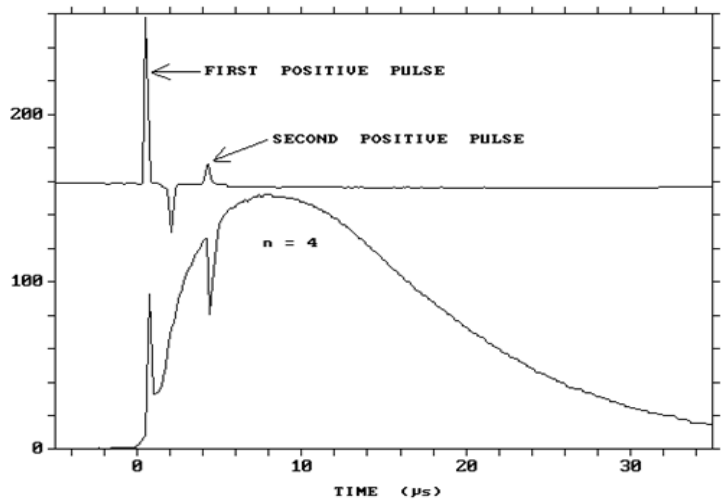

Fig. 6 – Quenching effect on H_β line in neon afterglow plasma.

Another proof of the recombination process that occurs in the temporal afterglow plasma was the radiative recombination continuum getting in the emission spectrum of cesium high voltage pulsed discharge afterglow plasma. The experimental set up was presented in details in [18]. The tube with cesium vapors was mounted in a two-chamber oven. The vapor pressure was controlled from the lowest temperature point of the liquid cesium pellet, which lies in an appendix in the lowest part of the oven. The vapor pressure was determined from the reservoir temperature according to the Taylor-Langmuir relation [19] and changed by modifying the temperature of the reservoir. A simple discharge tube (Φ = 2 cm, l = 16 cm) with two electrodes mounted at a distance d = 13 cm between them, is placed in the upper part of the oven and maintained at a temperature at least 40 K greater than that of the cesium reservoir.

The atomic cesium emission spectra in the range of 410–550 nm during the current pulse and at different moments in the afterglow were recorded using the gate electronic system presented above. As it can be seen in Fig. 7, the emission lines of the sharp and diffuse series are broadened and merge together as they approach their series limits (6P). The merged lines at the series limit go smoothly into the intensive radiative recombination continuum which is seen on the blue side of the series limit, in the range 410–500 nm (that corresponds to about 0.37 eV). The band resulting from the free-bound transitions to the 6P states was used in the diagnosis of the cesium afterglow plasma more precisely in the determination of the electron temperature. This band is easily and unmistakably identifiable and is unencumbered by superimposed lines. The band head occurs at the series limits of prominent CsI line spectra. While it is possible to mention other processes yielding continua, such as bremsstrahlung, a sharp band head characterizes none of them.

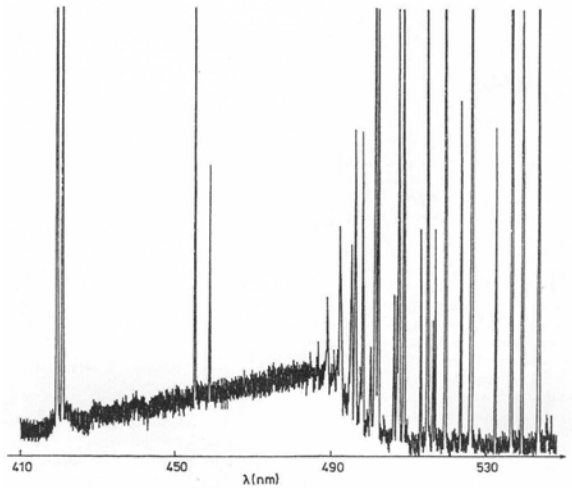

Fig. 7 – Emission spectrum of the cesium afterglow plasma in the range 410–550 nm recorded with an electronic gate of 8 μs widths, opened at 10 μs after the end of the voltage pulse.

The use of the radiative recombination continuum in the electron temperature determination in cesium afterglow plasma depends upon the condition that the electron velocity distribution is maxwellized, a condition which is guaranteed by the rapid electron-electron thermalization in the afterglow plasma. One of the advantages of this spectroscopic diagnostics method is that only relative spectral intensities need to be known in order to get electron temperatures.

Few words about the procedure for determining the electron temperature. In the radiative recombination process $Cs^+ + e^- \rightarrow Cs + h\nu$, an atomic ion captures a free electron in one, let say j, of the discrete bound atomic states and a single photon is released with the energy $h\nu = hc/\lambda = hc/\lambda_j + mv^2/2$, where hc/λ_j is the binding energy of the bound state j and $mv^2/2$ is the kinetic energy of the free electron. This process, occurring within plasma, yields distinctive spectral bands, each limited on the low energy side by a band head corresponding to the binding energy of a specific atomic state. The intensity distribution for the band associated with the j^{th} state is given by:

$$I_j(\lambda)\mathrm{d}\lambda = (hc/\lambda)R_j(\lambda)\mathrm{d}\lambda = (hc/\lambda)N_eN_iv\sigma_j(v)F(v)\mathrm{d}v\,, \qquad (3.2.1)$$

where $R_j(\lambda)$ is the rate of photon emission in the interval $\mathrm{d}\lambda$ corresponding to the electron velocity in the range $\mathrm{d}v$; N_e and N_i are the electron, respectively cesium ion concentrations; $\sigma_j(v)$ is the radiative recombination cross section for an electron of velocity v to make transition to the state j; $F(v)\mathrm{d}v$ is the fraction of electrons in the range $\mathrm{d}v$. The electron temperature T_e, enters in $F(v)\mathrm{d}v$, which is assumed to be Maxwellian. Substituting the Maxwell distribution function in (1), we get

$$I_j(\lambda)\mathrm{d}\lambda = \left(\frac{2m}{\pi}\right)^{1/2} \frac{h^2c^2}{(kT_e)^{3/2}} \frac{N_e N_i v^2 \sigma_j(v)}{\lambda^3} \exp\left[-\frac{hc}{kT_e}(\lambda^{-1} - \lambda_j^{-1})\right]\mathrm{d}\lambda\,. \quad (3.2.2)$$

Using further the expression for $\sigma_j(v) = 3\times10^{-56}\lambda^2/mv^2h^2c^2$, as calculated by Mohler [20], and taking the logarithm, the final equation becomes

$$\ln[\lambda I(\lambda)] = \text{const.} - (hc/kT_e)(1/\lambda). \quad (3.2.3)$$

Plotting ln[λI(λ)] *versus* 1/λ by making relative intensity measurements at 10 wavelengths upon the band shape, the experimental points (Fig. 8) follow a straight line, sustaining the assumption concerning the Maxwellian distribution function of electrons.

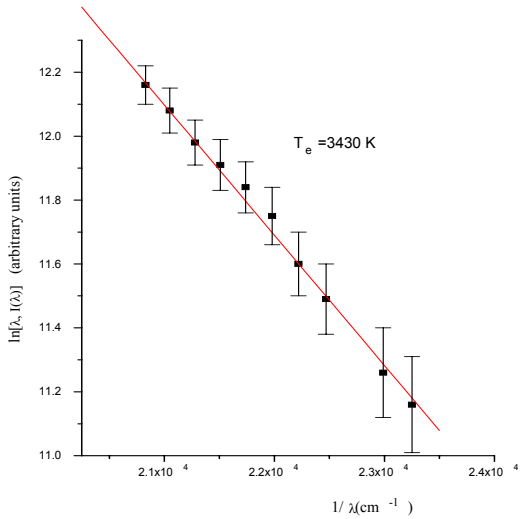

Fig. 8 – Experimental graph ln[λI(λ)] = *f*(1/λ) and the fitting line.

According to equation (3), the slope of the straight-line gives for the presented experimental conditions an electron temperature $T_e \approx 3430$ K with an estimated error of about 30 K (the variation of the electron temperature in the temporal range 10–50 μs is included in the measurement errors) [21].

3.3. PROCESSES BEHIND THE UNCOMMON TEMPORAL PROFILES OF ATOMIC AND IONIC SPECTRAL LINES IN TEMPORAL AFTERGLOW PLASMAS

Sometimes for the elucidation of the uncommon temporal profiles of the population of atomic or ionic energy levels theoretical models may help. Thus, in

the case of long afterglow duration (more than 100 μs) of the Balmer lines observed in helium and neon hollow cathode pulsed discharge, accompanied by a population inversion between the $n = 3$ and $n = 4$, 5, 6 levels of the hydrogen atom (Fig. 9), we proposed a theoretical model [4, 22] based on the assumption that the Penning ionization of hydrogen molecules by collisions with noble gas metastable atoms is followed by selective production of excited atomic hydrogen by dissociative recombination of the molecular hydrogen ion. The proposed model agrees with the experimental temporal profiles (shape and size) of hydrogen impurity level populations in helium and neon afterglow.

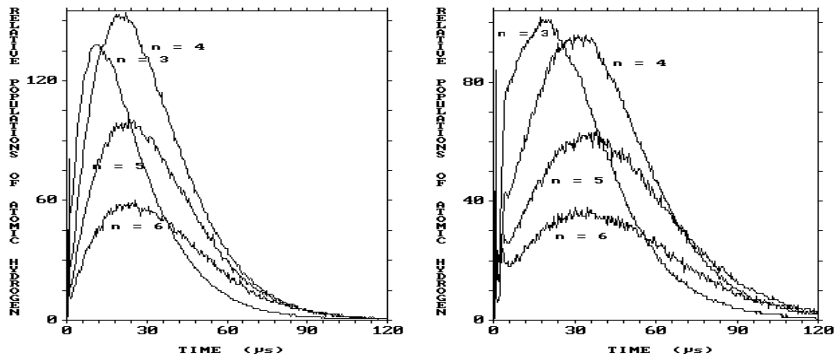

Fig. 9 – Relative population of atomic hydrogen levels in: a) He afterglow; b) neon afterglow.

In the helium afterglow plasma of the hollow cathode pulsed high voltage discharge we shall consider the Penning ionization of hydrogen molecules, hydrogen being as impurity in the plasma

$$He^m + H_2 \longrightarrow He + H_2^+ + e_{slow} \tag{3.3.1}$$

and the metastable ionization

$$He^m + He^m \longrightarrow He^+ + He + e_{fast}\,. \tag{3.3.2}$$

Since the excitation energy of helium metastable atoms is 19.8 eV and the ionization energy of the hydrogen molecule is 15.9 eV, electrons produced in reaction (3.3.1) have a kinetic energy of about 3.9 eV (or 0.7 eV in the case of neon). From similar considerations we get that electrons produced in reaction (3.3.2) have a kinetic energy of about 15 eV (or 11.7 eV in the case of neon). Such electrons, which we call "slow" or "fast" respectively, are continuously produced during the afterglow, though they quickly lose their initial energy by recoil impacts with noble gas atoms.

Adopting the assumption of Dezenberg and Willett [23], that hydrogen atomic levels are populated by electron-ion dissociative recombination, i.e.

$$H_2^+ + e \longrightarrow H_2^* \longrightarrow H + H^* \ (n = 3, 4, 5), \tag{3.3.3}$$

where only low vibrational states of hydrogen molecular ions are available for recombination with electrons, because higher excited vibrational states are removed by exothermic reactions with noble gas atoms [24]. Taking into account the gain by recombination processes and the loss by spontaneous emission, the rate equation of atomic hydrogen population, N, has the form

$$dN_n / dt = \alpha_n n_i n_s + \beta_n n_i n_f - A_n N_n, \tag{3.3.4}$$

where: n_i, n_s, n_f denote concentrations of molecular hydrogen ions, and of slow and fast electrons, respectively; α_n, β_n are recombination coefficients for slow and fast electrons, respectively, associated with the n^{th} level of the hydrogen atom; A_n is the corresponding radiative decay frequency. In fact, $A_n > 10^7$ s^{-1} and, for the afterglow time scale, $dN_n/dt << A_n N_n$, thus (3.3.4) becomes

$$N_n = (1/A_n)(\alpha_n n_i n_s + \beta_n n_i n_f). \tag{3.3.5}$$

As can be seen from the equations (3.3.1) and (3.3.2) the concentrations n_i, n_s, n_f, as functions of time depend on the concentration of metastables which continuously decrease during the afterglow due to loss processes as diffusion and deactivation on noble gas atoms and on molecular hydrogen impurities (under our experimental conditions, the last process appears to be the most important). We shall assume that the temporal profile of the metastable concentration has an exponential decay

$$M = M_o \exp(-t/\tau_m), \tag{3.3.6}$$

with the initial concentration M_0 and the time constant τ_m.

The H_2^+ molecular ion distribution

$$\partial n_i l \partial t = -n_i l \tau_i + \nu_p M, \tag{3.3.7}$$

where τ_i is the time constant for ambipolar diffusion and ν_p the Penning ionization frequency has the solution

$$n_i(t) = \nu_p M_0 F_{i,m}(t), \tag{3.3.8}$$

where $F_{i,m}$ is defined by

$$F_{i,m}(t) = \frac{\exp(-t/\tau_i) - \exp(-t/\tau_m)}{(1/\tau_m) - (1/\tau_i)}. \tag{3.3.9}$$

Similar considerations are valid for the slow electron group, produced by Penning ionization, with the only difference that the ion time constant, τ_i, is replaced by the slow electron time constant, τ_s, i.e.

$$n_s(t) = \nu_p M_o F_{s,m}(t)\,, \tag{3.3.10}$$

where the function $F_{s,m}(t)$ has the same form as defined by (3.3.9). Finally, the fast electron group, produced by metastable-metastable ionization, can be considered in the same manner. However, the corresponding rate equation contains a gain rate of quadratic form, CM^2, instead of the linear term, $\nu_p M$. Consequently, the fast electron concentration has the expression

$$n_f(t) = CM_o^2 F_{f,2m}(t)\,. \tag{3.3.11}$$

Thus the final expression for the equation (3.3.5) is

$$N_n(t) = F_{i,m}(t)\left[P_n F_{s,m}(t) + Q_n F_{f,2m}(t)\right], \tag{3.3.12}$$

where $F(t)$ is the unique function defined by (3.3.9) and the constants

$$P_n = \left(\alpha_n / A_n\right)\nu_p^2 M_0^2 \quad \text{and} \quad Q_n = (\beta_n / A_n) C \nu_p M_o^3 \tag{3.3.13}$$

play the role of scaling factors.

In spite of the simplicity of the theoretical model set forth in the preceding paragraph, (3.3.12) fits rather well the experimental data concerning the relative populations of atomic hydrogen impurities in helium and neon afterglow. This agreement is illustrated in Fig. 10 and the resulting fitting time constants are $\tau_i = 55.56$ μs; $\tau_s = 8.33$ μs; $\tau_f = 2.27$ μs.

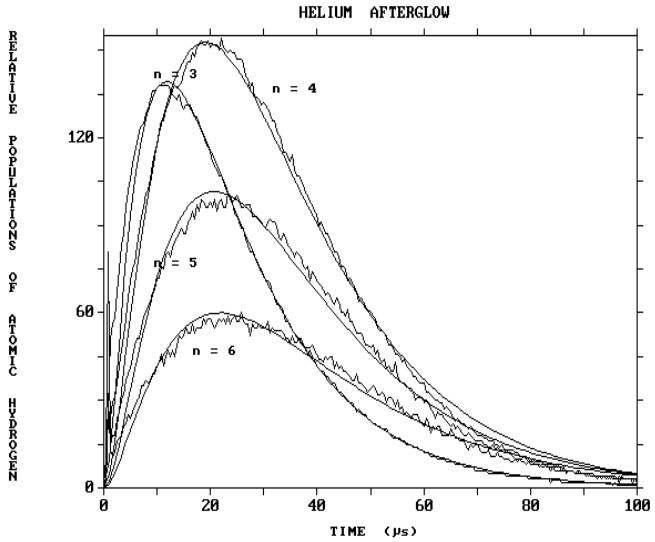

Fig. 10 – Relative population of atomic hydrogen levels in helium afterglow and the fitting curves obtained by the theoretical proposed model.

From the diffusion theory we got $T_f/T_s \cong \tau_s/\tau_f$ when T_f, T_s>>T. The obtained fitting data give $T_f/T_s \cong \tau_s/\tau_f = 8.33/2.27 \cong 3.7$. On the other side, the ratio of kinetic energies of electrons produced in ionization reactions is $E_f/E_s = 15/3.9 \cong 3.8$, where E_s is the slow electron energy, (3.3.1), and E_f the fast electron energy, (3.3.2).

Using the experimental data obtained in neon-hydrogen mixtures and the theoretical model presented above, a simple method for the determination of partial pressure of hydrogen impurities in the neon afterglow was proposed [25].

Other uncommon temporal profiles of the light emitted by the temporal afterglow plasma were the profiles of NeII, ArII and XeII spectral lines emitted in the early afterglow of pulsed high voltage hollow cathode discharge (Fig. 11).

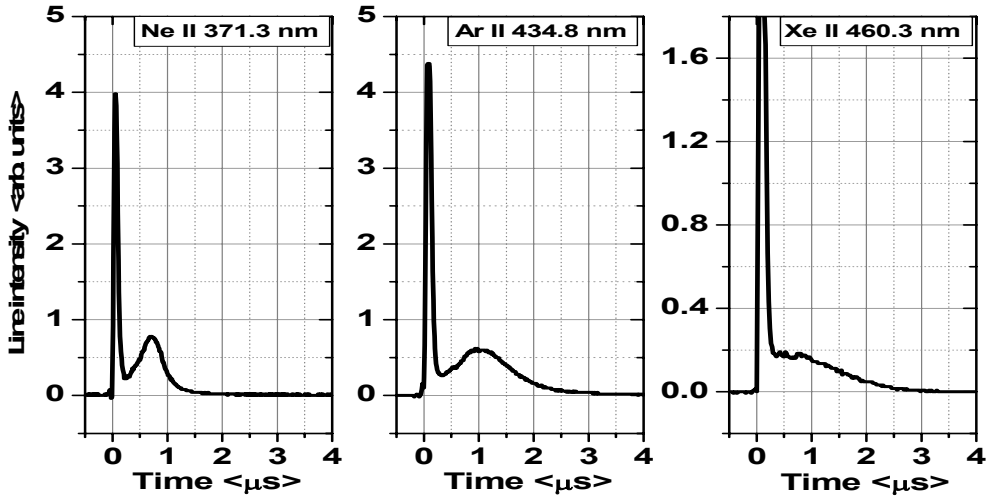

Fig. 11 – Temporal profiles of spectral lines Ne II, ArII and Xe II.

Elucidating the mechanism of ion levels population required further spectral investigations and was based on previous results acquired by applying the theoretical model to the hydrogen levels population in noble gas pulsed discharge [4]. Thus the spectra recorded with a variable electronic gate positioned during the current pulse and during the hump leads to the conclusion that during the hump period the energy levels of ions are mainly populated by recombination of double-ionized ions, in contrast to the current (discharge) period, when ions excitation is caused by impact with energetic electrons. The recombination processes may lead even to a population inversion as it can be seen (Fig. 12) in the case of the Ar II energy levels 4p $^4D_{7/2}$ (19.49 eV) and 5s $^4P_{5/2}$ (22.51 eV).

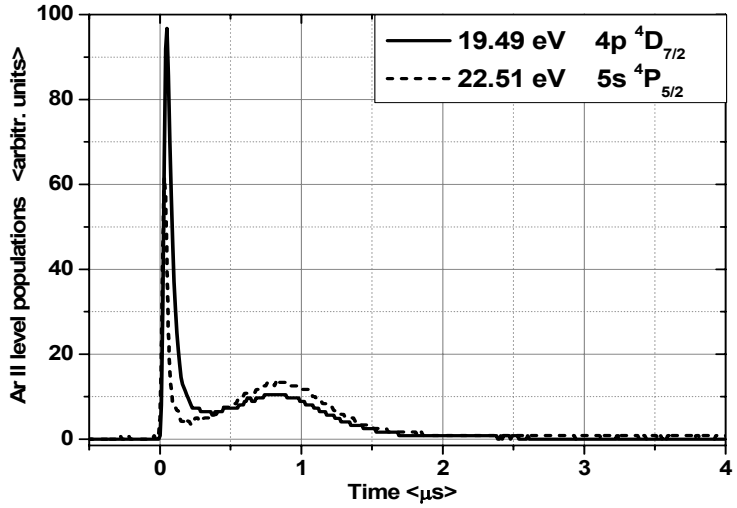

Fig. 12 – Population inversion of ArII energy levels: 4p $^4D_{7/2}$ (19.49 eV) and 5s $^4P_{5/2}$ (22.51 eV).

We presumed that in the afterglow of the high current hollow cathode pulsed discharge the energy levels of the noble gases ions, are populated by the following mechanism

$$A^{++} + e + M \rightarrow A^{+*} + M, \tag{3.3.14}$$

where A^{++} is generated by

$$A^{m} + A^{+m} \rightarrow A^{++} + e. \tag{3.3.15}$$

In order to sustain our supposition regarding the process (2), additional investigation of the temporal evolution the Ne, Ar and Xe ionic lines in the presence of controlled hydrogen traces.

Thus, the previous papers [4] showed that in the afterglow of the pulsed discharges in neon the metastable atoms are responsible for levels population of the hydrogen impurities *via* processes ($Ne^m + H_2 \rightarrow Ne + H_2^+ + e$, $\sigma = 2.65\times10^{-16}$ cm^2 [26], $H_2^+ + e \rightarrow H_2^* \rightarrow H^*$ (n = 6, 5, 4, 3) + H). Similarly, in argon afterglow plasma the metastable ions are involved in the population process of hydrogen impurity energy levels ($Ar^{+m} + H_2 \rightarrow Ar^m + H_2^+$, $\sigma = 3.6\times10^{-16}$ cm^2 [27], $H_2^+ + e \rightarrow H_2^* \rightarrow H^*$ (n = 6, 5, 4, 3) +H).

Figure 13 presents the temporal evolution of Ne II 3713 Å line and H_β line of hydrogen in a pulsed discharge in neon (5 Torr) with hydrogen traces at partial pressures 7×10^{-2} Torr (dashed line) and 1.2×10^{-1} Torr (solid line), for the same experimental conditions.

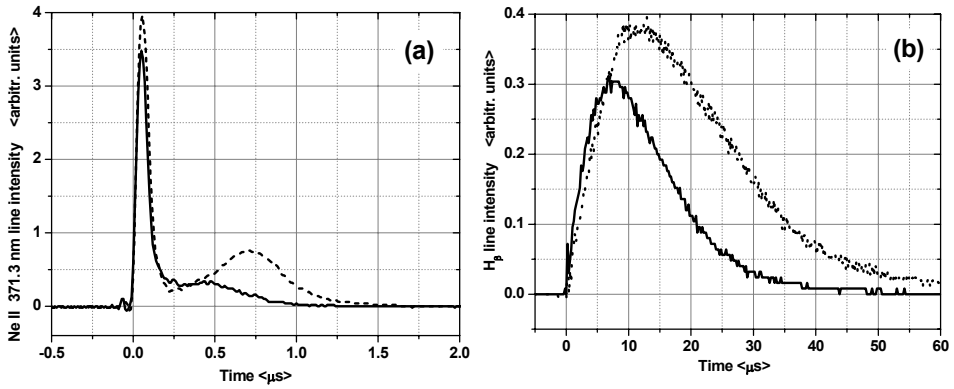

Fig. 13 – Temporal evolution of 3713 Å Ne II line (a) and H_β line (b), for hydrogen partial pressures: 7×10^{-2} Torr – dashed line, respectively 1.2×10^{-1} Torr – solid line.

The above figures show that the increase of hydrogen concentration influences in the same way the temporal evolution of both, the H_β line and ionic hump, namely the peaks decrease and shift toward earlier afterglow. In the two cases this behavior is due to the intensification of neon atom metastable destruction by Penning effect ($Ne^m + H_2 \rightarrow Ne + H_2^+ + e$), with increasing the hydrogen concentration. Thus we may say that the noble gas metastable atoms are involved in the generation of the ionic hump in the temporal afterglow.

The time evolution of Ar II line at 4348 Å and H_β line emitted from pulsed discharges in argon (1.3 Torr) with hydrogen impurities at partial pressures 7×10^{-2} Torr (dashed line), respectively 1.2×10^{-1} Torr (solid line) are presented in Fig. 14.

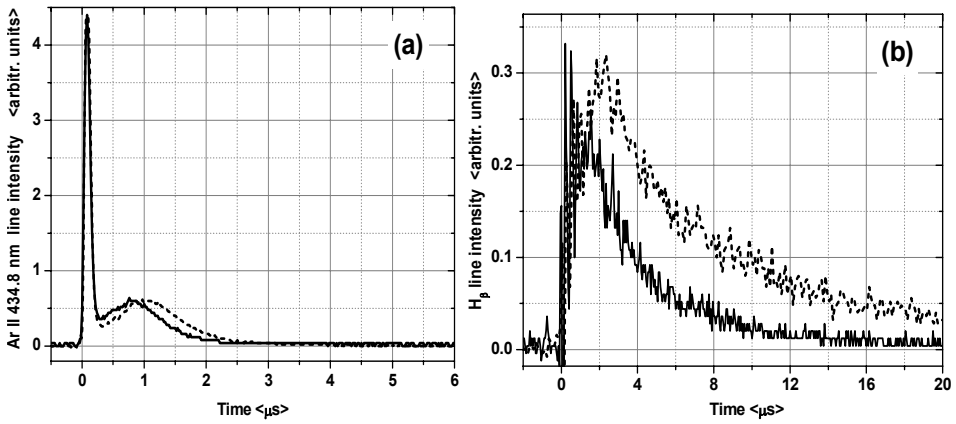

Fig. 14 – Temporal evolution of 4348 Å Ar II line (a) and H_β line (b), for hydrogen partial pressures: 7×10^{-2} torr – dashed line, respective 1.2×10^{-1} torr – solid line.

Like in the neon case, the changes of hydrogen concentration, affect in the same way the ionic hump and H_β line. Nevertheless, the argon case is somehow different because the temporal evolution of the argon metastable ions is affected by the Penning effect, not the metastable atoms. We may say in this case that metastable ions are involved in the generation of the hump in the temporal profile of the ionic lines in afterglow. In Xenon there is no Penning effect on hydrogen molecules, neither on metastable atoms nor metastable ions. The temporal evolution of Xe II 4603 Å line in xenon discharge at 1 Torr remains unchanged when hydrogen is added and the H_β line do not appear at all in the afterglow. This fact represents a further argument sustaining the population mechanism of ionic energy levels responsible for the amplification of ionic lines in the afterglow of noble gases.

4. CONCLUSIONS

The spectral investigation of the temporal afterglow plasma of short high voltage pulsed discharges in noble gases allows the development of new diagnostic methods for these plasma such as the gas temperature determination from the frequency of the shock waves and electron temperature determination from the continuum radiative recombination.

The simple theoretical model proposed to elucidation from the temporal profile of the spectral lines the mechanism of the atomic levels population agrees with the experimental data and sustain the existence in the afterglow plasma of two groups of electrons able to produce excitations and ionizations after the end of the current pulse.

The spectral investigation in the presented specific plasma configuration provided evidence that the large number of atomic and ionic metastables act like a real ionization source for the sputter analyte atoms and for atoms and ions of buffer gas in the temporal afterglow of analytical plasma. Studies of processes involving atomic and ionic metastables are of great interest, since they should lead to a better control over the ionization mechanisms crucial to analytical glow discharge mass spectrometry (GDMS) analysis.

Acknowledgements. This work is supported by UEFISCDI projects with the following codes: PN II –ID-PCE-2011-3-0958 and PT-PCCA-2011-3.1-1136.

REFERENCES

1. M.Ganciu, A.Surmeian, C.Diplasu, I.Chera, G.Musa, I.I.Popescu, Opt. Commun., **88**, 381 (1992).
2. C.Diplasu, A.Surmeian, A.Groza, M.Ganciu, Surface and Coatings Technologies, **203**, 2858–2862 (2009).
3. Deloche R, Monchicourt P, Cheret M, Lambert F, Phys. Rev. A, **13**, 1140 (1976).
4. A.Surmeian, C.Diplasu, I.I.Popescu, C.B.Collins, *SPIE*, **2461**, 10 (1995).

5. A. Surmeian, C. Diplasu, C.B. Collins, G. Musa, I. Iovitz Popescu, Rom. J. of Physics, **41**, 661, (1996).
6. A.Surmeian, C. Diplasu, A. Groza, M. Ganciu**,** Rom. Reports Phys., **60**, 3, 609–614 (2008).
7. A. Groza, A. Surmeian, C. Diplasu, D. Vinteler, M. Ganciu, Rom. J. Phys., **56**, 83–89 (2011).
8. A. Surmeian, C. Diplasu, A. Groza, M. Ganciu, P. Bellanger, A. Tempez, P. Chapon, Analytical and Bioanalytical Chemistry, **388**, 8, 1625–1629 (2007).
9. J. B. Hasted, *Physics of Atomic Collisions*, 2nd edition, American Elsevier Publishing Company, Inc. 1972, Ch. 7.
10. A. Surmeian, C. Diplasu, C. B. Collins, G. Musa, I-Iovitz Popescu, J. Phys. D: Appl. Phys., **30,** 1341 (1997).
11. G. K. Born, R. G. Buser, J. of Appl. Phys., **37**, 4918 (1966).
12. Lord Rayleigh, *The Theory of sound*, Vol. II, Macmillan, London, 1996, pp. 267 and 298 1896.
13. A. Surmeian, C. Diplasu, C.B. Collins, G. Musa, I.-Iovitz Popescu, Rom. Reports. Phys., **49**, 183 (1997).
14. A. Surmeian, C. Diplasu, A. Groza, R. Stoian, M. Ganciu, I.-Iovitz Popescu, Journal of Optoelectronics and Advanced Materials, **7**, *4*, 2183–2188 2005.
15. A Surmeian, C Diplasu, A Groza, M Ganciu, P Chapon, I Iovitz Popescu, Optoelectr. Adv. Materials – Rapid Communication, **12**, *11*, 2311–2314 (2010).
16. A. Surmeian, C. Diplasu, A. Groza, A. Tempez, P.C hapon, M. Ganciu, ESCAMPIG 2012, Portugal.
17. C.L. Chen, C.C. Leiby, and L. Goldstein, Phys. Rev., **121**, 1391 (1961).
18. A. Surmeian, C. Diplasu, C. B. Collins, G. Musa, I-Iovitz Popescu, J. Phys.D: Appl.Phys., **30,** 1755 (1997).
19. Taylor J. and Langmuir I., Phys. Rev., **51**, 753 (1937).
20. Mohler F.L., Rev. Mod. Phys., **1**, 216 (1929).
21. A. Surmeian, C. Diplasu, C.B. Collins, G. Musa, I.-Iovitz Popescu, Rom. Reports Phys., **49,** 189 (1997).
22. A. Surmeian, C. Diplasu, C.B. Collins, G. Musa, I.-Iovitz Popescu, Rom. J. Phys., **41,** 661 (1996).
23. G.J. Dezenberg, C.S. Willett, IEEE J.OE-7, **10**, 491 (1971).
24. Amarjit Sen, J.W. McGowan, J.B.A. Mitchell, J. Phys. B: At. Mol. Phys., **20**, 1509 (1987).
25. A. Surmeian, C. Diplasu, C.B. Collins, G. Musa, I. -Iovitz Popescu, Rom. Reports in Physics, **49**, 575 (1997).
26. A. Ricard, J. de Physique, **38**, C3- 239 (1977).
27. K. Kadota, Y. Kaneko, J. Phys. Soc. Jpn., **38**, 524 (1975).